Magnet Measurements for the FET Recirculation Experiment

J. Karn, N. Sereno

January 13, 1992

1 Introduction

The measurents performed on the magnets used in the Front End Test (FET) recirculation experiment[1,4] are described. The magnets consist of 9 dipole and 14 quadrupole magnets from the University of Illinois, 4 CEBAF linac (QB) quadrupoles, 3 energy recovery chicane dipoles constructed at CEBAF, and a small corrector dipole also constructed at CEBAF. The injecton chicane dipoles are not described in this note. The magnets have been assigned positions in the beamline[5] based on measurements made at CEBAF and the requirements of the beamline optics. This note describes the measurements made on the magnets using the rotating coil technique[2,3] and lists the data for each magnet in a table at the end. The goal of the measurement is to obtain the integrated multipole coefficient along the magnet (beam) axis for the dipoles and quadrupoles as a function of current. The apparatus used in these measurements was developed at CEBAF for measurement of the magnets to be used in the linacs and arcs of the CEBAF recirculating linac.

2 The Rotating Coil Measurement

The basic measurement apparatus shown in figure 1 is a coil of thin wire consisting of N turns mounted on a rigid frame that is made to rotate in a magnetic field which can be expanded in terms of multipole coefficients (dipole, quadrupole, sextupole etc.). In cylindrical coordinates the magnetic field after integration over z is given by,[2,3]

$$\begin{aligned} B_r(r,\vartheta) &= \sum_{n=1}^{\infty} B_n r^{n-1} \sin(n\vartheta - \alpha_n) \\ B_\vartheta(r,\vartheta) &= \sum_{n=1}^{\infty} B_n r^{n-1} \cos(n\vartheta - \alpha_n), \end{aligned} \tag{1}$$

where n is the multipole index ($n = 1$ is the dipole contribution to the field, $n = 2$ is the quadrupole contribution, etc.), B_n is the multipole coefficient, and α_n is an angle that gives the orientation of the multipole relative to the cylindrical coordinate system. The coil rotates in the rz plane such that $\vartheta = \omega_o t$, and generates an emf according to Faraday's law that is a sum of terms corresponding

to each of the multipole coefficients B_n. Furthermore, each term has a sinusoidal time dependence of frequency $n\omega_o$ where ω_o is the angular velocity of the coil in radians per second. Fourier analysis of the emf generated by the coil results in a line spectrum where the amplitude of each line is proportional to the integral of the multipole coefficient along the z axis of the coil (the nominal direction that the electron beam passes through the magnet).

2.1 Dipole and Quadrupole Emf Signals from the Rotating Coil

Specifically, the dipole ($n = 1$) and quadrupole ($n = 2$) emf signals in the spectrum are given by,

$$\mathcal{F}\left(\int_0^t \mathcal{E}_1(t')dt'\right) = N(r_1 + r_2)\int_{-l/2}^{l/2} B_1 dz \tag{2}$$

$$\mathcal{F}\left(\int_0^t \mathcal{E}_2(t')dt'\right) = (N/2)(r_1^2 - r_2^2)\int_{-l/2}^{l/2} B_2 dz \tag{3}$$

$$0 \le t \le 2\pi/\omega_o,$$

where $\mathcal{F}$ denotes the Fourier Transform, ω_o is the angular frequency of rotation of the coil probe, $\mathcal{E}_1$ and $\mathcal{E}_2$ are the emf generated by the dipole (B_1) and quadrupole (B_2) contributions to the field, N is the number of coil turns, r_1 and r_2 are the distance of each coil wire from the center of rotation and l is the length of the coil probe. Equations 2 and 3 are the basis for calibrating the coil probes for an absolute measure of the dominant integrated multipole coefficient for each dipole and quadrupole magnet.

2.2 Measurement Apparatus and Procedure

The measurements are made with an apparatus consisting of a coil probe aligned along the magnetic symmetry axis of the multipole magnet under study (for these measurements either a dipole or a quadrupole) as shown in figure 1. A computer readout and control system spins the coil using a stepping motor, processes the coil emf signal, and changes the electric current of the multipole magnet in a preprogrammed hysteresis cycle. First, the control system adjustes the current in the magnet and rotates the coil at a constant angular frequency ω_o. During the rotation the emf signal is electronically integrated and Fourier analyzed using a Fast Fourier Transform (FFT). For each current, five rotations of the coil are made and the average of the five rotations of the output of the FFT (in $\mu V \cdot s$) is calculated for each of the multipole coefficients B_n up to $n = 10$ for the particular magnet under study. Values for α_n are also calculated for each multipole up to $n = 10$ and the results are tabulated in a data file.

3 Calibration of the Coil Probes

The parameters of the two coil probes used the measurements are listed in table 1. The smaller probe ($r_1 = 1.118$ cm) denoted as coil 1, was used to measure the dipole magnets which have an aperture of 1.27 cm and the large probe ($r_1 = 2.4613$ cm) denoted as coil 2, was used to measure the quadrupole magnets which have an aperture of 3.3 cm. The coil used to measure each magnet was chosen to fill as much of the magnet's available aperture as possible so as to produce the largest

emf signal. The coil probes are calibrated by spinning them in a dipole field that has been measured with a hall probe along the magnet axis. The output of the readout electronics gives the integrated emf generated by the coil so that the dipole coil constant in equation 2 can be measured directly. Using the measured dipole constant of the coil the quadrupole coil constant in equation 3 can be determined.

3.1 Calibration of the Coil Probe for Measurement of a Dipole Field

Using equation 2 the dipole constant of the coil can be defined as,

$$K_D = \frac{\int_{-l/2}^{l/2} B_1 dz}{\mathcal{F}\left(\int_0^t \mathcal{E}_1(t')dt'\right)}. \tag{4}$$

The calibration procedure consists of measuring the magnetic field of a dipole magnet using a hall probe at various values of z along the magnet and then numerically integrating the field data along z so that the numerator in equation 4 can be determined. The coil probe to be calibrated is then rotated in the magnet such that its center of rotation is placed on the hall probes measurement axis so that the denominator of equation 4 is the output from the FFT. The constant K_D can therefore be experimentally determined for each coil. Care must be taken so that the measurement of the field integral with the hall probe and the coil probe rotation measurement are performed at the same point on the magnets hysteresis curve. The theoretical value of the constant K_D is determined by inspection of equation 2,

$$K_D = \frac{1}{N(r_1 + r_2)}. \tag{5}$$

Equation 5 can be used as a check of the value of K_D determined from experiment. The dipole constant determines the dipole field (B_1) integral per unit integrated dipole emf ($\mathcal{E}_1$). Once K_D is known for the probe, the probe can be used to determine the integrated dipole coefficient for an unknown dipole magnet by performing a rotation and multiplying the integrated emf (the output of the FFT) by K_D.

3.2 Determination of the Calibration Dipole Field Integral

Figure 2 shows the hall probe data for the calibration dipole. The calibration magnet was first cycled around a hysteresis curve between ± 10 amperes 3 times and then the current was set at 5.0 amperes. The hall probe data and the coil probe data were taken at this same point on the hysteresis curve. The hall probe was mounted on a moveable sled and the calibration magnet was placed in the center of the travel of the sled. From the data in figure 2, the center of magnetic symmetry along the z axis is at about $z = 25$ cm. The data points were taken every .5 cm until the end of the travel of the sled was reached. The midpoint of the coil probe was also placed at $z = 25$ cm when it was rotated to record the integrated dipole emf. From the data points in figure 2, the major portion of the field integral was determined using standard numerical techniques. The curves for $z < 0.0$ cm and $z > 53.0$ cm were determined by a least squares fit to the data for the first and last 15 data points measured with the hall probe. The fitted function,

$$B_1(z) = \frac{a}{(z-b)^3}, \tag{6}$$

is the functional form for a dipole field where a and b are parameters to be determined from the least squares fit. Table 2 lists the relavant parameters of the least squares fit including χ^2 which was determined assuming an rms error of the field points of .5 Gauss (roughly the value of the earths field). The area under the curve given by equation 6 for $z > 53.0$ cm and $z < 0.0$ cm is obtained by integration using the fitted parameters from table 2. This small additional area is added to the field integral numerically calculated because the coil probe extends beyond the measured data where there is still a small dipole field which can contribute to the integrated emf. The endpoints of the integration are slightly different for each probe because each is a different length and each was centered in the calibration dipole. Table 3 lists K_D for both coil probes and compares the measured value to the theoretical value using equation 5 and the constants of the probe.

3.3 Coil Probe Dipole Constant Error Analysis

The percent error in the value of K_D for each coil was determined by adding the estimated percent errors of the numerator and denominator of equation 4 in quadrature according to,

$$\frac{\Delta K_D}{K_D} = \sqrt{\left(\frac{\Delta I_{B_1}}{I_{B_1}}\right)^2 + \left(\frac{\Delta I_{\mathcal{E}_1}}{I_{\mathcal{E}_1}}\right)^2} \tag{7}$$

$$I_{B_1} = \int_{-l/2}^{l/2} B_1 dz \tag{8}$$

$$I_{\mathcal{E}_1} = \mathcal{F}\left(\int_0^t \mathcal{E}_1(t')dt'\right). \tag{9}$$

The error in the value of the dipole field integral (equation 8) was determined by considering the .5 Gauss magnetic field of the earth which contributes to the field integral along the length of the coil probe outside the magnet. The error in the integrated emf (equation 9) was estimated from the variance in ten sets of rotations (a set being five rotations as described in §2.2). The average of the 10 sets of rotations was taken to be the integrated emf used to calculate K_D. The error in the integrated emf was found to be $(\frac{\Delta I_{\mathcal{E}_1}}{I_{\mathcal{E}_1}})$ only .02% compared to the error in the field integral $(\frac{\Delta I_{B_1}}{I_{B_1}})$ of 1.8% for coil 1 and 1% for coil 2. K_D is therefore limited by the error in the measurement of the field integral. Table 3 shows good agreement between the theoretical value of K_D and the measured value. The results of table 3 are used to calibrate the coil probes for their response to a quadrupole field.

3.4 Calibration of the Coil Probe for Measurement of a Quadrupole Field

The quadrupole constant for the probe K_Q is defined analogous to K_D,

$$K_Q = \frac{\int_{-l/2}^{l/2} B_2 dz}{\mathcal{F}\left(\int_0^t \mathcal{E}_2(t')dt'\right)}, \tag{10}$$

where the numerator of equation 10 is determined by measuring a quadrupole field and then rotating the coil in the field to determine the denominator. The quadrupole constant defined in equation 10 determines the quadrupole gradient (B_2) integral per unit integrated quadrupole emf

($\mathcal{E}_2$). Determination of K_Q by use of equation 10 is complicated by difficulties in measuring the quadrupole field with a hall probe directly. K_Q can be determined indirectly by dividing equation 3 by equation 2 which results in a formula for K_Q in terms of the measured dipole constant of the coil K_D, and the coil parameters r_1 and r_2,

$$K_Q = \frac{2K_D}{r_1 - r_2}. \tag{11}$$

The measurement of K_D for the coil therefore implies a straightforward determination of K_Q for the coil. Table 4 list the value of K_Q for both coil probes used in these measurements.

3.5 Coil Probe Quadrupole Constant Error Analysis

From equation 11, the uncertainty in K_Q is due to the uncertainties in both the dipole constant of the coil K_D and the coil parameters r_1 and r_2. The uncertainty in K_Q was determined by adding in quadrature both of these uncertainties,

$$\frac{\Delta K_Q}{K_Q} = \sqrt{\left(\frac{\Delta K_D}{K_D}\right)^2 + 2\left(\frac{\Delta r}{r_1 - r_2}\right)^2}, \tag{12}$$

where Δr is the uncertainty in the coil parameters r_1 and r_2. The coil parameters r_1 and r_2 actually measure distances to the center of each coil bundle where each bundle has a width d as shown in figure 1. It has been shown[6] that a coil consisting of a bundle of N turns geometrically behaves as a single turn coil where the effective radii extend from the center of rotation to the center of the bundle (figure 1). For a well constructed coil support, Δr is of the order of .2 mm. Coil 2 was chosen for the quadrupole measurement because it nearly filled the available quadrupole aperture thereby producing the largest emf signal and $\frac{\Delta r}{r_1 - r_2}$ was smaller than the corresponding ratio for coil 1.

4 FET Dipole and Quadrupole Data

The final data sheets list the values of the integrated multipole coefficient for the dipoles and quadrupoles using the calibrated coil probes 1 and 2. All magnets were measured at various currents around the hysteresis curve that they will be operated in the recirculation experiment. At each current, the field at the center of each dipole was also measured with a hall probe so that the effective length of the dipoles could be determined,

$$L_{ef} = \frac{\int_{-l/2}^{l/2} B_1 dz}{B_1^c}. \tag{13}$$

B_1^c in equation 13 is the central field measured with a hall probe. The effective length of the University of Illinois dipoles was found to be 19 cm consistently for all the dipoles at each current with small saturation effects observed at the highest currents. The two types of CEBAF energy recovery chicane dipoles were found to have effective lengths of 18.5 cm and 36.8 cm respectively. The small CEBAF corrector dipole for the first 180 degree bend was found to have an effective length of 22.5 cm. The effective length of the University of Illinois quadrupoles can be taken to

be the length of the pole piece which is roughly 20 cm. The CEBAF linac (QB) quads have pole pieces of 15 cm and therefore an effective length of 15 cm. The percent error in the dipole and quadrupole multipole integral values in the tables can be taken to be the percent error in the dipole and quadrupole constants for the coils listed in tables 3 and 4. The percent error in L_{ef} can be taken to be the error in the field integral (the numerator in equation 13) and hence the error in K_D for coil 1. The final graphs of this note show plots of the central field (B_1^c), field integral ($\int_{-l/2}^{l/2} B_1 dz$), and effective length (L_{ef}) versus current for Illinois dipole 1 and the gradient integral ($\int_{-l/2}^{l/2}, B_2 dz$) versus current for Illinois quadrupole 1 as examples of what the data look like when plotted. The data for the other dipoles and quadrupoles is similar. The Illinois dipole data show saturation at currents above about 60 amperes and typical hysteresis phenomena. The Illinois quadrupole data and CEBAF dipole and quadrupole data show no saturation up to 10 amperes but do show hysteresis. The Illinois dipoles are numbered from 1 to 9, the Illinois quadrupoles are numbered from 1 to 14, and the CEBAF energy recovery chicane dipoles are numbered from 1 to 3. The small CEBAF corrector dipole for the first 180 degree bend is labeled with the number 4. The beamline name for each magnet is also listed in the data tables for all the dipoles and quadrupoles that are used in the recirculation experiment.

5 Acknowledgement

The authors would like to thank L. Harwood for many helpful comments and suggestions during the course of these measurements.

References

[1] W. Barry, J. J. Bisognano, L. S. Cardman, J. Kewisch, G. A. Krafft, N. S. Sereno, C. K. Sinclair, *A Proposal for Accelerator Physics Experiments Using a Beam Recirculated Through the Front-End-Test Accelerator at CEBAF*, CEBAF-TN-90-231, 1990.

[2] J. Cobb, R. Cole, *Proceedings of the International Symposium on Magnet Technology*, SLAC, 431, 1965.

[3] G. E. Fischer, *Iron Dominated Magnets*, Physics of Particle Accelerators, AIP Conference Proceedings 153, SLAC, 1120, 1985.

[4] N. Sereno, *Accelerator Physics Experiments Using a Beam Recirculated through the Injection Accelerator at CEBAF*, CEBAF-TN-90-282, 1991.

[5] N. Sereno, *Magnet Placement for the FET Recirculation Experiment*, CEBAF-TN-91-053, 1991.

[6] C. Wyss, *A Measuring System for Magnets With Cylindrical Symmetry*, Fifth International Conference on Magnet Technology (MT-5) Rome-Italy, 231, 1975.

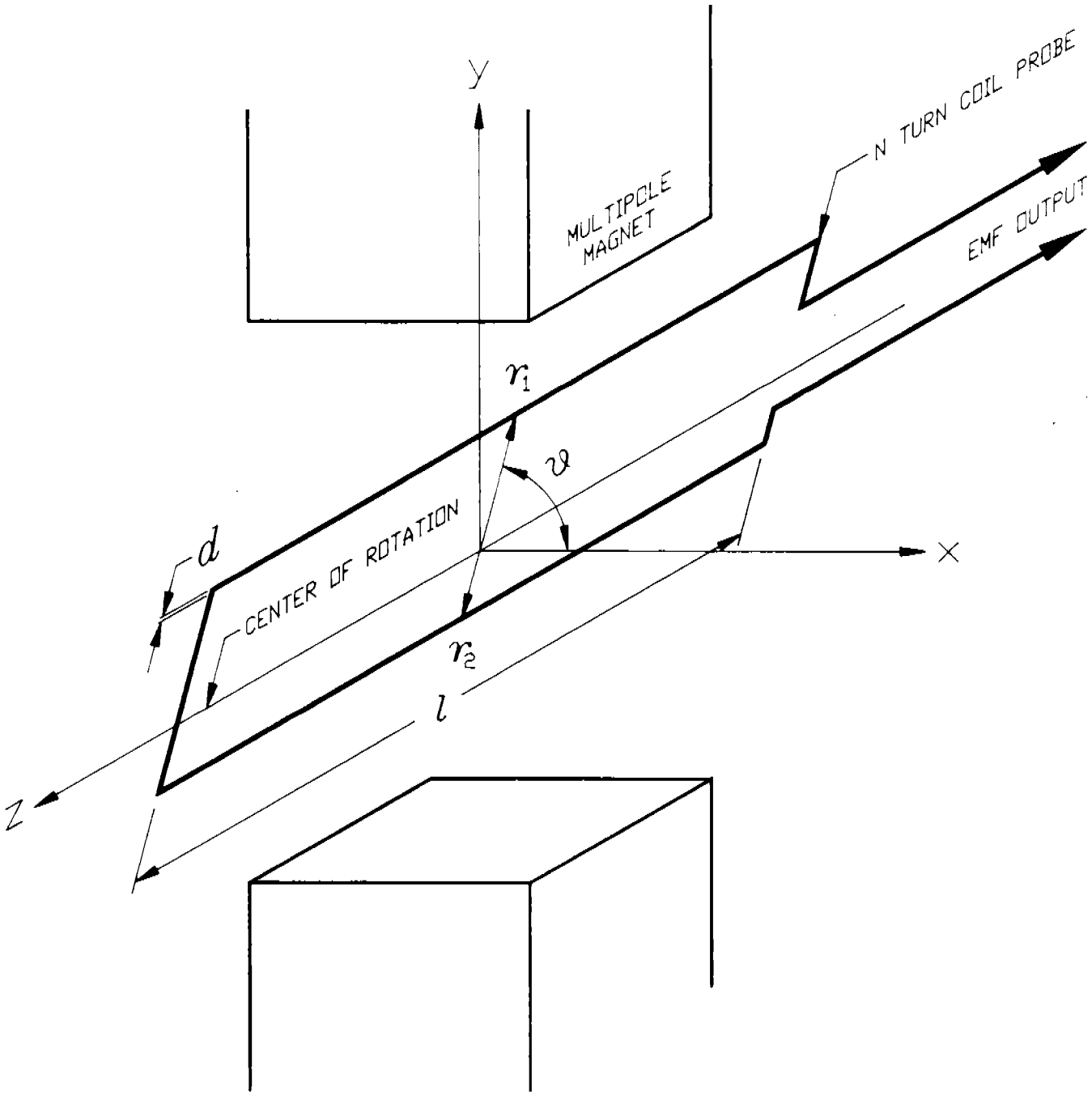

Figure 1: The rotating coil probe measurement scheme.

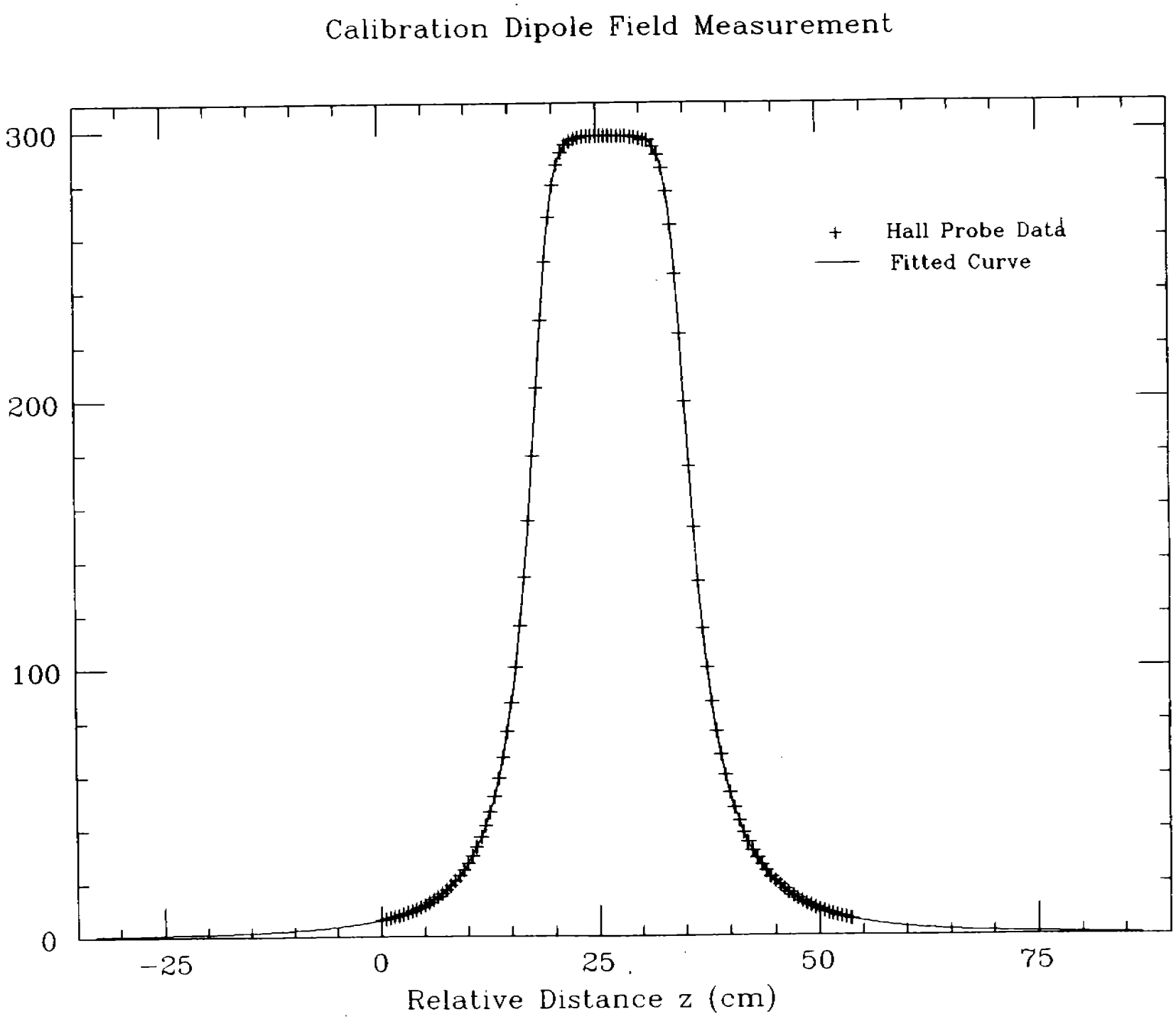

Figure 2: Magnetic field vs distance for the calibration dipole.

Table 1: Coil probe parameters.

Coil #	N	r_1 (cm)	r_2 (cm)	d (cm)
1	47	1.118	0.559	0.091
2	49	2.461	1.288	0.091

Table 2: Values of the least squares fit parameters.

Region of z axis (cm)	a (Gauss·cm^3)	b (cm)	χ^2
< 0.0	-1.11 $\times 10^5$	26.01	2.2 $\times 10^{-2}$
> 53.0	1.08 $\times 10^5$	27.62	7.8 $\times 10^{-2}$

Table 3: K_D for the coil probes.

Coil #	K_D (m^{-1}) (measured)	Relative Error $\frac{\Delta K_D}{K_D}$ %	$K_D = \frac{1}{N(r_1+r_2)}$ (m^{-1}) (theory)
1	1.312 $\pm$ .024	1.8	1.269
2	0.548 $\pm$ .005	1.0	0.544

Table 4: K_Q for the coil probes.

Coil #	K_Q (m^{-2}) (measured)	Relative Error $\frac{\Delta K_Q}{K_Q}$ %	$K_Q = \frac{2}{N(r_1^2-r_2^2)}$ (m^{-2}) (theory)
1	469 $\pm$ 25	5.4	454
2	93.4 $\pm$ 2.4	2.6	92.7

Table 1: University of Illinois dipole magnet data.

Magnet	Dipole 1			Dipole 2		
Beamline Name	BNRB10			BNRB05		
Current (amperes)	B_1^c (kGauss)	$\int_{-l/2}^{l/2} B_1 dz$ (kGauss·cm)	L_{ef} (cm)	B_1^c (kGauss)	$\int_{-l/2}^{l/2} B_1 dz$ (kGauss·cm)	L_{ef} (cm)
0	.017	.403	23.2	.018	.422	23.5
10	.742	-	-	.736	-	-
20	1.477	28.490	19.3	1.467	28.165	19.2
30	2.215	-	-	2.196	-	-
40	2.944	56.649	19.2	2.919	55.753	19.1
50	3.668	-	-	3.636	-	-
60	4.384	84.097	19.2	4.344	82.970	19.1
70	5.082	97.408	19.2	5.029	96.054	19.1
80	5.702	109.00	19.1	5.653	107.41	19.0
90	6.228	118.72	19.1	6.184	116.88	18.9
100	6.689	127.04	19.0	6.649	125.67	18.9
90	6.244	119.07	19.1	6.201	117.82	19.0
80	5.732	109.66	19.1	5.686	108.03	19.0
70	5.115	98.207	19.2	5.069	96.818	19.1
60	4.422	84.741	19.2	4.375	84.002	19.2
50	3.697	-	-	3.665	-	-
40	2.968	57.092	19.2	2.943	56.506	19.2
30	2.240	-	-	2.218	-	-
20	1.498	28.810	19.2	1.486	28.531	19.2
10	.756	-	-	.752	-	-
0	.0174	.404	23.2	.018	.434	24.1

Magnet	Dipole 3			Dipole 4		
Beamline Name	BNRB06			BNRB08		
Current (amperes)	B_1^c (kGauss)	$\int_{-l/2}^{l/2} B_1 dz$ (kGauss·cm)	L_{ef} (cm)	B_1^c (kGauss)	$\int_{-l/2}^{l/2} B_1 dz$ (kGauss·cm)	L_{ef} (cm)
0	.016	.412	26.4	.017	.412	24.8
10	.747	-	-	.745	-	-
20	1.478	28.476	19.3	1.482	28.609	19.3
30	2.215	-	-	2.219	-	-
40	2.949	56.724	19.2	2.955	56.956	19.3
50	3.677	-	-	3.681	-	-
60	4.390	84.304	19.2	4.395	84.538	19.2
70	5.083	97.643	19.2	5.086	97.788	19.2
80	5.706	109.21	19.1	5.699	109.19	19.2
90	6.225	118.85	19.1	6.212	118.70	19.1
100	6.685	127.11	19.0	6.665	126.81	19.0
90	6.242	119.20	19.1	6.228	119.05	19.1
80	5.736	109.89	19.2	5.730	109.90	19.2
70	5.127	98.479	19.2	5.130	98.666	19.3
60	4.424	84.963	19.2	4.432	85.243	19.2
50	3.701	-	-	3.712	-	-
40	2.970	57.200	19.3	2.980	57.439	19.3
30	2.233	-	-	2.242	-	-
20	1.497	28.844	19.3	1.504	28.980	19.3
10	.7525	-	-	.757	-	-
0	.016	.413	26.2	.017	.415	25.1

Magnet	Dipole 5			Dipole 6		
Beamline Name	BNRB04			BNRB13		
Current (amperes)	B_1^c (kGauss)	$\int_{-l/2}^{l/2} B_1 dz$ (kGauss-cm)	L_{ef} (cm)	B_1^c (kGauss)	$\int_{-l/2}^{l/2} B_1 dz$ (kGauss-cm)	L_{ef} (cm)
0	.014	.397	28.7	.017	.420	24.7
10	.743	-	-	.737	-	-
20	1.477	28.450	19.3	1.467	28.202	19.2
30	2.216	-	-	2.192	-	-
40	2.949	56.661	19.2	2.911	55.956	19.2
50	3.675	-	-	3.626	-	-
60	4.394	84.161	19.2	4.328	82.836	19.1
70	5.085	97.476	19.2	5.002	95.934	19.2
80	5.702	109.00	19.1	5.636	107.73	19.1
90	6.224	118.63	19.1	6.175	117.76	19.1
100	6.677	126.79	19.0	6.641	126.21	19.0
90	6.238	118.97	19.1	6.194	118.16	19.1
80	5.737	109.73	19.1	5.672	107.12	18.9
70	5.123	98.329	19.2	5.040	96.655	19.2
60	4.424	84.851	19.2	4.357	83.452	19.2
50	3.700	-	-	3.654	-	-
40	2.973	57.144	19.2	2.937	56.475	19.2
30	2.236	-	-	2.217	-	-
20	1.500	28.819	19.2	1.485	28.582	19.2
10	.756	-	-	.751	-	-
0 .	014	.398	28.0	.018	.422	24.0

Magnet	Dipole 7			Dipole 8		
Beamline Name	BNRB11			BNRB09		
Current (amperes)	B_1^c (kGauss)	$\int_{-l/2}^{l/2} B_1 dz$ (kGauss·cm)	L_{ef} (cm)	B_1^c (kGauss)	$\int_{-l/2}^{l/2} B_1 dz$ (kGauss·cm)	L_{ef} (cm)
0	.017	.408	23.4	.017	.417	24.0
10	.746	-	-	.750	-	-
20	1.474	28.416	19.3	1.485	28.516	19.2
30	2.210	-	-	2.219	-	-
40	2.943	56.617	19.2	2.955	56.830	19.2
50	3.665	-	-	3.677	-	-
60	4.384	84.123	19.2	4.398	84.408	19.2
70	5.073	96.524	19.0	5.087	97.729	19.2
80	5.691	107.20	18.8	5.702	109.21	19.2
90	6.208	118.50	19.1	6.223	118.85	19.1
100	6.661	124.65	18.7	6.677	127.11	19.0
90	6.223	118.84	19.1	6.241	119.21	19.1
80	5.724	109.67	19.2	5.738	109.93	19.2
70	5.116	98.314	19.2	5.129	98.613	19.2
60	4.418	84.825	19.2	4.435	85.126	19.2
50	3.695	-	-	3.709	-	-
40	2.965	56.535	19.1	2.977	57.343	19.3
30	2.235	-	-	2.241	-	-
20	1.496	28.795	19.2	1.501	28.914	19.3
10	.756	-	-	.759	-	-
0 .	017	.410	24.1	.017	.419	25.1

Magnet	Dipole 9		
Beamline Name	BNRB07		
Current (amperes)	B_1^c (kGauss)	$\int_{-l/2}^{l/2} B_1 dz$ (kGauss·cm)	L_{ef} (cm)
0	.019	.427	22.2
10	.747	-	-
20	1.484	28.476	19.2
30	2.225	-	-
40	2.954	56.736	19.2
50	3.684	-	-
60	4.405	84.299	19.1
70	5.101	97.627	19.1
80	5.718	109.21	19.1
90	6.236	118.85	19.1
100	6.695	127.13	19.0
90	6.254	119.24	19.1
80	5.747	109.95	19.1
70	5.140	98.556	19.2
60	4.438	85.051	19.2
50	3.714	-	-
40	2.978	56.650	19.0
30	2.245	-	-
20	1.503	28.377	18.9
10	.762	-	-
0	.018	.435	23.9

Table 1: CEBAF energy recovery chicane dipole magnet measurements.

Magnet	Dipole 1			Dipole 2		
Beamline Name	BNRB01			BNRB02		
Current (amperes)	B_1^c (kGauss)	$\int_{-l/2}^{l/2} B_1 dz$ (kGauss·cm)	L_{ef} (cm)	B_1^c (kGauss)	$\int_{-l/2}^{l/2} B_1 dz$ (kGauss·cm)	L_{ef} (cm)
0	.015	.257	17.2	.020	.685	34.6
1	.332	5.758	17.3	.326	11.905	36.6
2	.653	11.893	18.2	.642	23.589	36.7
3	.973	17.859	18.4	.957	35.216	36.8
3.5	-	-	-	1.114	40.985	36.8
4	1.296	23.745	18.3	1.270	46.727	36.8
4.5	-	-	-	1.425	52.445	36.8
4	1.296	23.745	18.3	1.282	47.121	36.8
3.5	-	-	-	1.130	41.548	36.8
3	.984	18.024	18.3	.976	35.906	36.8
2	.665	12.105	18.2	.662	24.305	36.7
1	.341	6.168	18.1	.343	12.481	36.4
0	.016	.260	16.5	.019	.690	36.3

Magnet	Dipole 3		
Beamline Name	BNRB03		
Current (amperes)	B_1^c (kGauss)	$\int_{-l/2}^{l/2} B_1 dz$ (kGauss·cm)	L_{ef} (cm)
0	.014	.301	21.5
1	.324	6.046	18.7
2	.639	11.982	18.7
3	.952	17.875	18.8
4	1.264	23.605	18.7
3	.963	18.054	18.7
2	.651	12.154	18.7
1	.335	6.244	18.7
0	.015	.310	20.6

Table 1: First 180 degree bend corrector dipole data.

Magnet	Dipole 4		
Beamline Name	BNRB12		
Current (amperes)	B_1^c (kGauss)	$\int_{-l/2}^{l/2} B_1 dz$ (kGauss·cm)	L_{ef} (cm)
0	-.005	-.195	39.7
1	.096	2.151	22.3
2	.196	4.409	22.5
3	.296	6.698	22.6
4	.396	8.954	22.6
3	.300	6.767	22.5
2	.202	4.562	22.5
1	.104	2.319	22.4
0	.004	.010	24.9
-1	-.097	-2.238	23.2
-2	-.197	-4.423	22.5
-3	-.297	-6.773	22.8
-4	-.397	-9.071	22.8
-3	-.301	-6.869	22.8
-2	-.203	-4.668	23.0
-1	-.105	-2.429	23.2
0	-.004	-.195	48.7

Table 1: University of Illinois quadrupole magnet data.

Magnet	Quadrupole 1	Quadrupole 2	Quadrupole 3	Quadrupole 4	Quadrupole 5
Beamline Name	QNRB06	QNRB01	QNRB07	QNRB14	QNRB03
Current (amperes)	$\int_{-l/2}^{l/2} B_2 dz$ (kGauss)				
0	.071	.075	.069	.068	.069
1	.655	.664	.649	.656	.660
2	1.270	1.280	1.266	1.275	1.277
3	1.887	1.903	1.882	1.897	1.900
4	2.514	2.528	2.507	2.525	2.529
5	3.138	3.159	3.132	3.154	3.157
6	3.769	3.790	3.755	3.787	3.789
7	4.398	4.420	4.382	4.415	4.423
8	5.027	5.054	5.014	5.045	5.058
9	5.651	5.684	5.641	5.681	5.686
10	6.284	6.318	6.265	6.317	6.318
9	5.693	5.724	5.678	5.718	5.725
8	5.074	5.110	5.070	5.099	5.110
7	4.454	4.487	4.448	4.478	4.490
6	3.831	3.858	3.824	3.850	3.856
5	3.204	3.227	3.195	3.219	3.226
4	2.573	2.599	2.566	2.586	2.591
3	1.946	1.962	1.942	1.957	1.959
2	1.318	1.330	1.316	1.324	1.326
1	0.692	.701	.692	.694	.697
0	.071	.075	.070	.069	.070

Magnet	Quadrupole 6	Quadrupole 7	Quadrupole 8	Quadrupole 9	Quadrupole 10
Beamline Name	QNRB02	QNRB08	*Not Used*	QNRB10	QNRB11
Current (amperes)	$\int_{-l/2}^{l/2} B_2 dz$ (kGauss)				
0	.071	.060	.062	.061	.071
1	.660	.686	.796	.676	.655
2	1.280	1.335	1.547	1.317	1.270
3	1.904	1.991	2.304	1.961	1.887
4	2.533	2.649	3.070	2.611	2.514
5	3.167	3.313	3.836	3.263	3.138
6	3.799	3.971	4.606	3.914	3.769
7	4.429	4.633	5.374	4.564	4.398
8	5.063	5.293	6.139	5.221	5.027
9	5.696	5.959	6.906	5.877	5.651
10	6.330	6.626	7.682	6.526	6.284
9	5.740	5.993	6.942	5.909	5.693
8	5.122	5.342	6.188	5.271	5.074
7	4.495	4.689	5.428	4.618	4.454
6	3.865	4.026	4.662	3.972	3.831
5	3.229	3.367	3.893	3.314	3.204
4	2.596	2.703	3.123	2.663	2.573
3	1.960	2.038	2.356	2.009	1.946
2	1.330	1.377	1.586	1.357	1.318
1	0.697	.716	.822	.707	.692
0	.071	.061	.063	.061	.071

Magnet	Quadrupole 11	Quadrupole 12	Quadrupole 13	Quadrupole 14
Beamline Name	QNRB09	QNRB16	QNRB15	*Not Used*
Current (amperes)	$\int_{-l/2}^{l/2} B_2 dz$ (kGauss)			
0	.066	.072	.066	.069
1	.675	.658	.662	1.018
2	1.314	1.274	1.280	1.993
3	1.958	1.894	1.904	2.980
4	2.601	2.524	2.535	3.974
5	3.261	3.154	3.165	4.965
6	3.914	3.785	3.802	5.959
7	4.561	4.411	4.435	6.953
8	5.218	5.049	5.062	7.941
9	5.875	5.678	5.698	8.940
10	6.532	6.310	6.332	-
9	5.913	5.718	5.731	8.940
8	5.279	5.099	5.118	7.987
7	4.628	4.476	4.487	7.014
6	3.977	3.853	3.857	6.013
5	3.321	3.222	3.225	5.026
4	2.668	2.592	2.593	4.033
3	2.014	1.959	1.957	3.039
2	1.365	1.325	1.325	2.043
1	0.716	.695	.692	1.051
0	.067	.072	.067	.070

Table 2: CEBAF Linac quadrupole (QB) data.

Magnet	QB001	QB102	QB103	QB104
Beamline Name	QBRB04	QBRB12	QBRB13	QBRB05
Current (amperes)	$\int_{-l/2}^{l/2} B_2 dz$ (kGauss)			
0	.247	.222	.235	.259
1	1.686	1.674	1.694	1.694
2	3.244	3.238	3.271	3.237
3	4.807	4.851	4.859	4.810
4	6.427	6.451	6.501	6.455
5	8.053	8.082	8.129	8.065
6	9.656	9.676	9.752	9.671
7	11.262	11.302	11.373	11.290
8	12.885	12.923	13.005	12.926
9	14.502	14.496	14.596	14.507
10	16.078	16.146	16.215	16.113
9	14.671	14.670	14.770	14.712
8	13.142	13.127	13.241	13.203
7	11.567	11.574	11.659	11.627
6	9.987	9.964	10.060	10.027
5	8.365	8.363	8.418	8.392
4	6.735	6.721	6.784	6.764
3	5.106	5.079	5.125	5.134
2	3.471	3.458	3.502	3.506
1	1.862	1.827	1.845	1.877
0	.248	.223	.235	.260

Bend Dipole Central Field

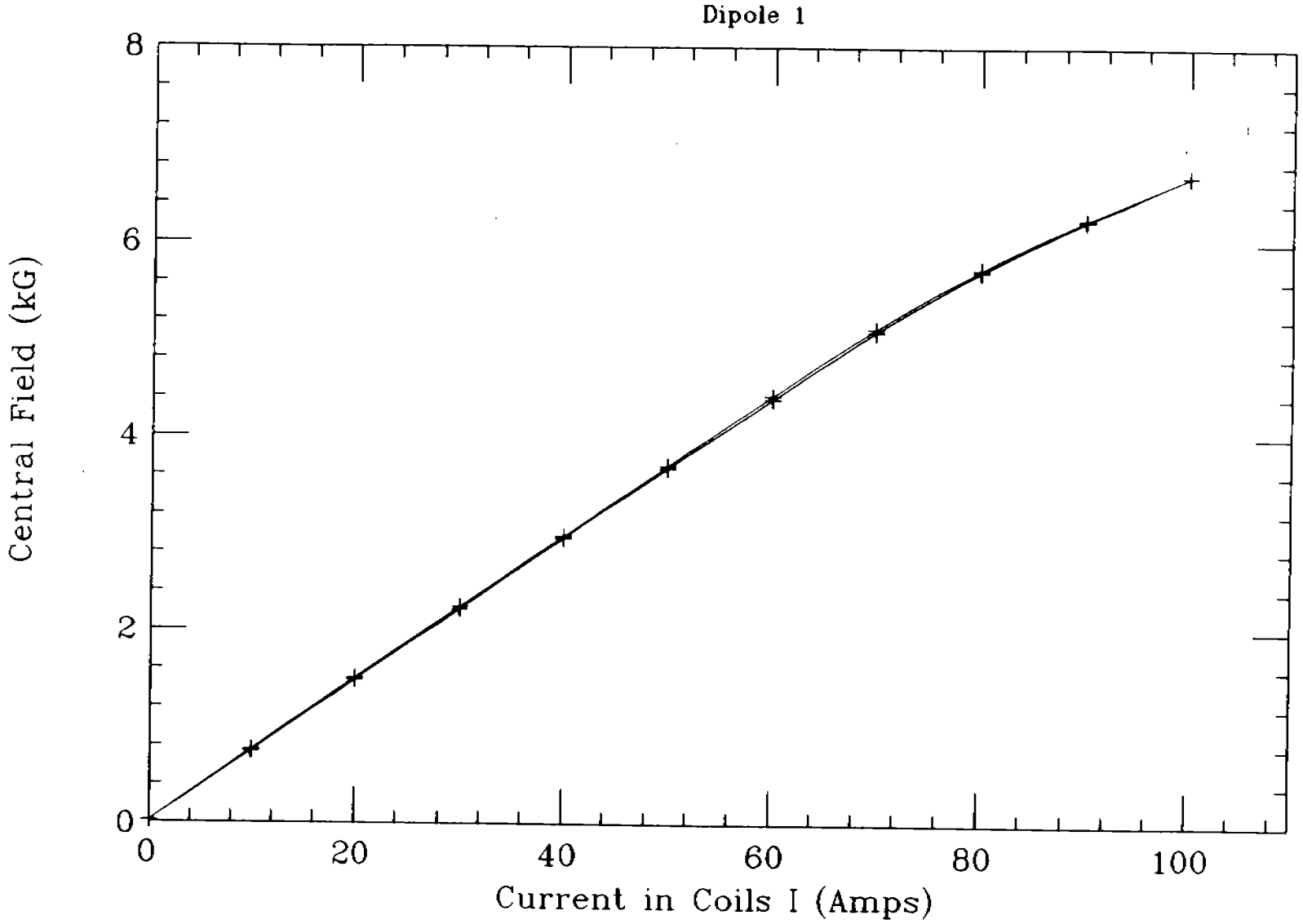

Bend Dipole Field Integral

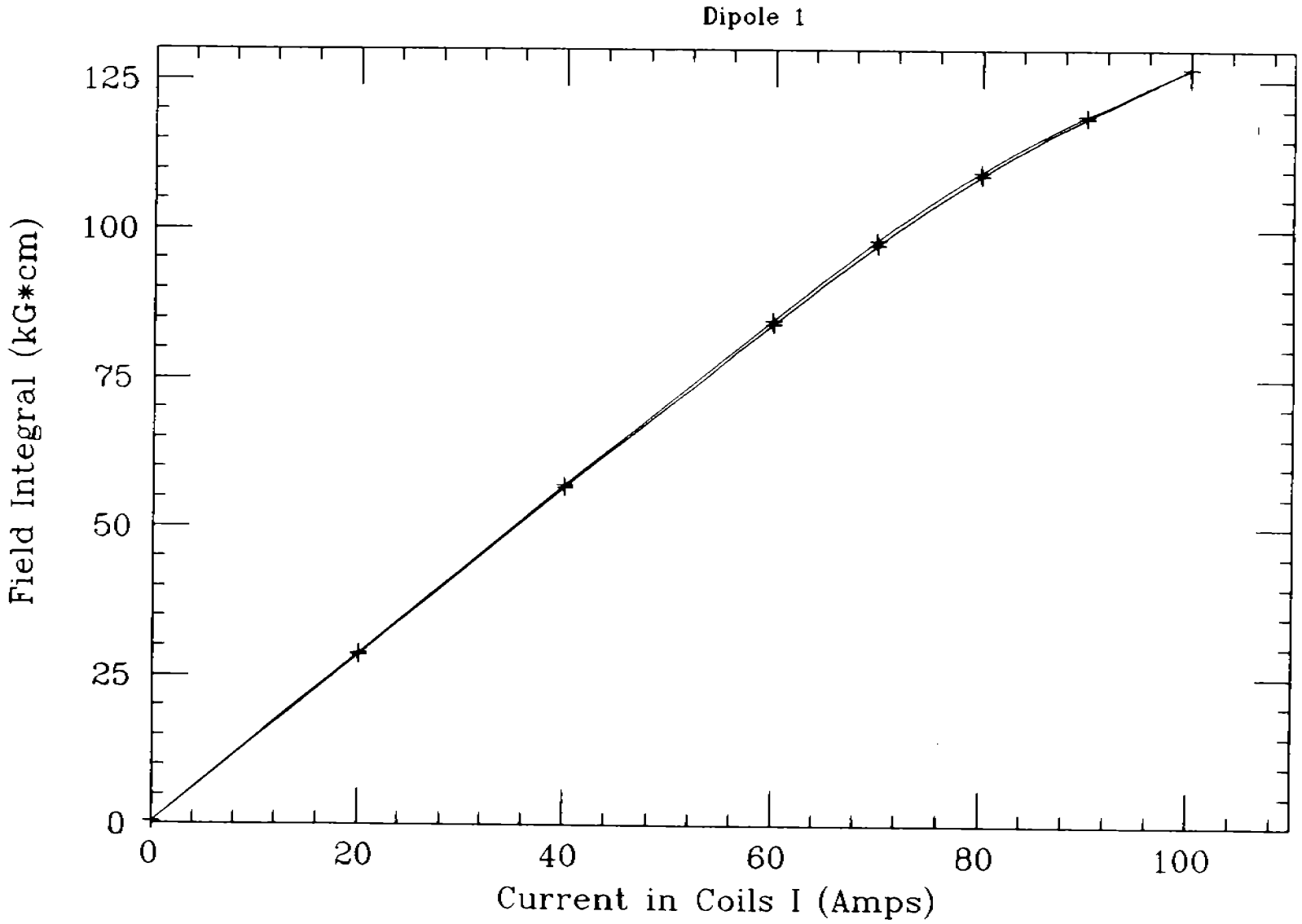

Bend Dipole Effective Length

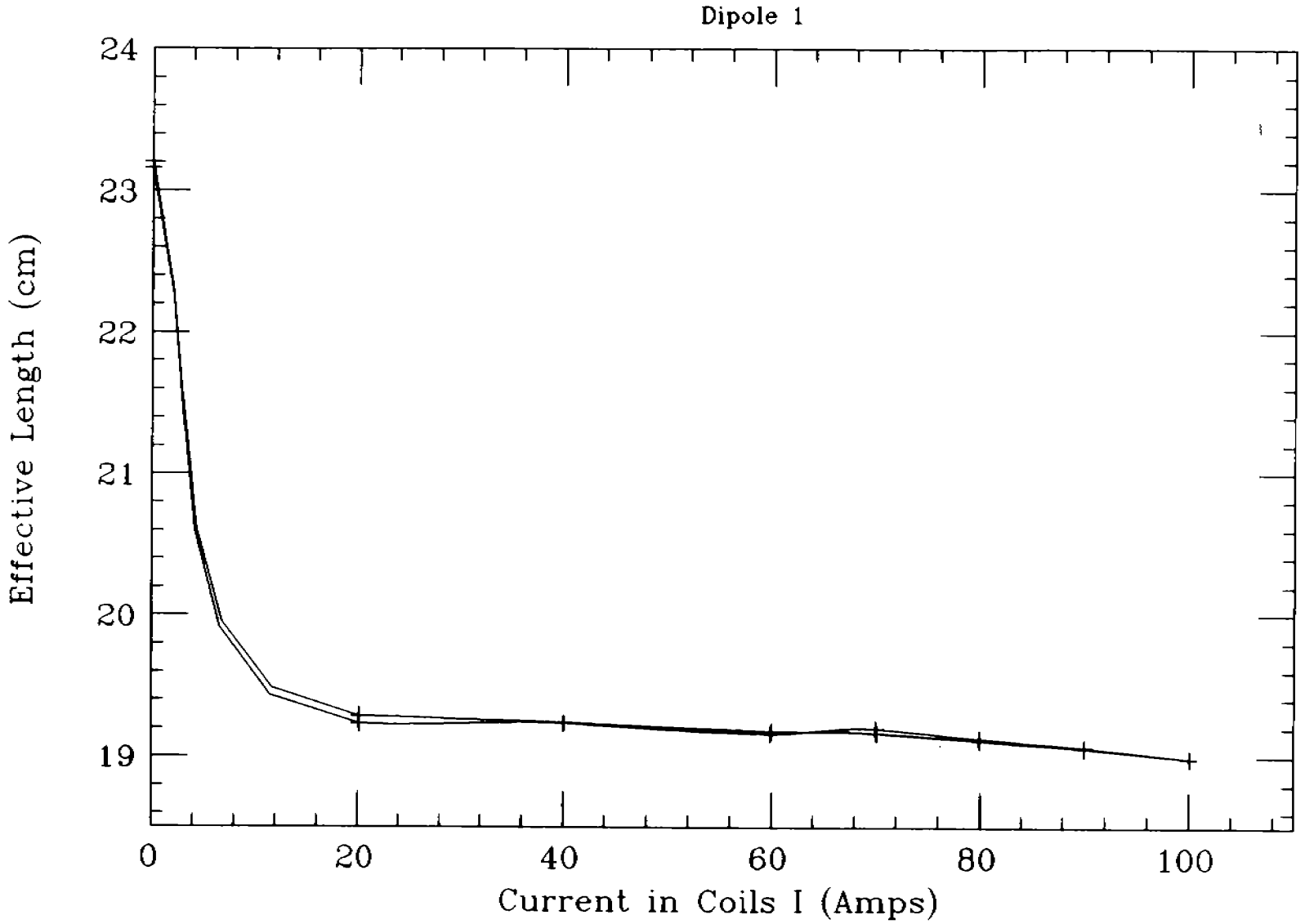

Quadrupole Field Gradient Integral